

Atomic Hong–Ou–Mandel experiment

R. Lopes¹, A. Imanaliev¹, A. Aspect¹, M. Cheneau¹, D. Boiron¹ & C. I. Westbrook¹

Two-particle interference is a fundamental feature of quantum mechanics, and is even less intuitive than wave–particle duality for a single particle. In this duality, classical concepts—wave or particle—are still referred to, and interference happens in ordinary space-time. On the other hand, two-particle interference takes place in a mathematical space that has no classical counterpart. Entanglement lies at the heart of this interference, as it does in the fundamental tests of quantum mechanics involving the violation of Bell’s inequalities^{1–4}. The Hong, Ou and Mandel experiment⁵ is a conceptually simpler situation, in which the interference between two-photon amplitudes also leads to behaviour impossible to describe using a simple classical model. Here we report the realization of the Hong, Ou and Mandel experiment using atoms instead of photons. We create a source that emits pairs of atoms, and cause one atom of each pair to enter one of the two input channels of a beam-splitter, and the other atom to enter the other input channel. When the atoms are spatially overlapped so that the two inputs are indistinguishable, the atoms always emerge together in one of the output channels. This result opens the way to testing Bell’s inequalities involving mechanical observables of massive particles, such as momentum, using methods inspired by quantum optics^{6,7}, and to testing theories of the quantum-to-classical transition^{8–11}. Our work also demonstrates a new way to benchmark non-classical atom sources^{12,13} that may be of interest for quantum information processing¹⁴ and quantum simulation¹⁵.

A pair of entangled particles is described by a state vector that cannot be factored as a product of two state vectors associated with each particle. Although entanglement does not require that the two particles be identical², it arises naturally in systems of indistinguishable particles owing to the symmetrization of the state, which leads to non-trivial, multiparticle interference. A remarkable illustration is the Hong, Ou and Mandel (HOM) experiment, in which two photons enter the two input channels of a 50:50 beam-splitter (one photon in each channel) and the correlation is measured between detectors at the two outputs.

A joint detection at these detectors arises from two possible processes: either both photons are transmitted by the beam-splitter or both are reflected (Fig. 1c). For two indistinguishable photons, both processes lead to the same final quantum state and the probability of joint detection results from the addition of their amplitudes. Because the beam-splitter corresponds to a unitary operation, these amplitudes have same modulus but opposite signs, thus their sum vanishes and so also the probability of joint detection^{16,17} (see also Methods). To be truly indistinguishable, not only must the photons have the same energy distribution and polarization, but their final spatio-temporal modes must be identical. Thus, the two photons must enter the beam-splitter in modes that are the exact images of each other. As a result, when measured as a function of the delay between the arrival times of the photons on the beam-splitter, the correlation exhibits the ‘HOM dip’, ideally going to zero at zero delay.

Our experiment is equivalent in all important respects to the HOM experiment, but is performed with bosonic atoms instead of photons. We produce freely propagating twin beams of metastable ⁴He atoms¹⁸, which we then reflect and overlap on a beam-splitter using Bragg scattering on an optical lattice (ref. 19 and Fig. 1). The photon counters

after the beam-splitter are replaced by a time-resolved, multi-pixel atom-counting detector²⁰, which enables the measurement of intensity correlations between the atom beams in well defined spatial and spectral regions. The temporal overlap between the atoms can be continuously tuned by changing the moment when the atomic beam-splitter is applied. We observe the HOM dip when the atoms simultaneously pass through the beam-splitter. The key technical advance that has enabled

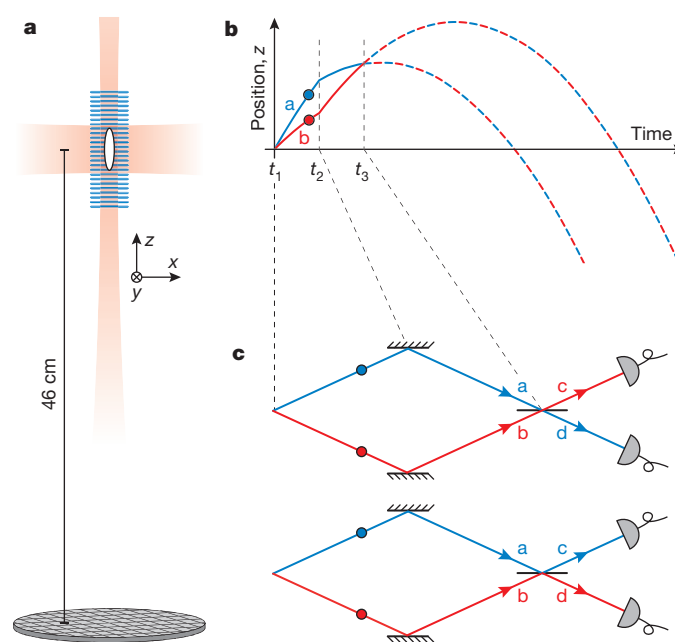


Figure 1 | Schematic of the experiment. **a**, A Bose–Einstein condensate (BEC, white oval) of metastable ⁴He atoms is trapped in an elongated optical trap (red shaded area). A moving optical lattice, here depicted in blue, is superimposed on the BEC and triggers the scattering of atom pairs along the *z* axis. When this lattice and the trap are switched off, the atoms fall towards a microchannel plate detector located 46 cm below the initial position of the BEC (drawing not to scale). **b**, The time diagram shows the evolution of the twin atoms’ vertical coordinates (blue line for beam *a* and red line for beam *b*). Between t_1 and t_2 , t_2 and t_3 , and after t_3 , the atoms move under the sole influence of gravity (drawing not to scale). At t_3 , the twin atom velocities are swapped using Bragg diffraction on an optical lattice. At time t_3 , when the atomic trajectories cross again, the same lattice is applied for half the amount of time in order to realize a beam-splitter. The lines alternately dashed in red and blue symbolize the indiscernibility of the atoms’ trajectories after the beam-splitter. The filled red and blue circles indicate the position of the atoms at a given time before the beam-splitter is applied. **c**, In the centre-of-mass frame of reference, the trajectories of the atoms resemble those of the photons in the Hong–Ou–Mandel experiment. A joint detection arises either when both atoms are transmitted through the beam-splitter (upper panel) or when both are reflected (lower panel). If the two particles are indistinguishable, these processes end in the same final quantum state and the probability of joint detection results from the addition of their amplitudes. For bosons these amplitudes have same modulus but opposite signs, thus their sum vanishes and so also does the probability of joint detection.

¹Laboratoire Charles Fabry, Institut d’Optique Graduate School – CNRS – Université Paris Sud, 2 avenue Augustin Fresnel, 91127 Palaiseau, France.

this work was the improvement of the atom pair production so as to permit optimal adjustment of the mode populations¹⁸.

We begin by producing a Bose–Einstein condensate (BEC) of metastable ⁴He atoms in the $1s2s\ ^3S_1$ internal state (here we represent this by $2\ ^3S_1$), with the projection of the total electronic angular momentum $m = 1$. The BEC contains $(5\text{--}6) \times 10^4$ atoms and is confined in an elliptical optical trap with its long axis along the vertical (z) direction (Fig. 1a). The atomic cloud has radii of 58 and 5 μm along the longitudinal (z) and transverse (\perp) directions, respectively. A moving optical lattice, superimposed on the BEC for 300 μs , induces the scattering of atom pairs (hereafter referred to as twin atoms) in the longitudinal direction through a process analogous to spontaneous four-wave mixing^{18,21,22} (see also Methods). This mixing process resembles that used in refs 23–25 to generate entangled states in the spin sector, but it involves the motional degrees of freedom. One beam, labelled a, has a free-space velocity $v_z \approx 12.1\text{ cm s}^{-1}$ in the laboratory frame of reference and the other beam, labelled b, has a velocity $v_z \approx 7.0\text{ cm s}^{-1}$ (Fig. 1b, c). The twin atom beams clearly appear in the velocity distribution of the atoms, which is displayed in Fig. 2. The visible difference in population between the beams is attributed to secondary scattering processes in the optical lattice, leading to the decay over time of the quasi-momentum states¹⁸. After the optical lattice has been switched off (at time t_1), the twin atoms propagate in the optical trap for 200 μs . At this moment, the trap itself is switched off and the atoms are transferred to the magnetically insensitive $m = 0$ internal state by a two-photon Raman transition (Methods).

From here on, the atoms evolve under the influence of gravity and continue to move apart (Fig. 1b). At time $t_2 = t_1 + 500\ \mu\text{s}$, we deflect the beams using Bragg diffraction on a second optical lattice, so as to make them converge. In the centre-of-mass frame of reference, this deflection reduces to a simple specular reflection (Fig. 1c and Methods). At time $t_3 \approx 2t_2 - t_1$, we apply the same diffraction lattice for half the amount of time in order to realize a beam-splitting operation on the

crossing atom beams. Changing the time t_3 allows us to tune the degree of temporal overlap between the twin atoms. Figure 1c shows the atomic trajectories in the centre-of-mass frame of reference and reveals the close analogy with a photonic HOM experiment.

The atoms end their fall on a microchannel plate detector located 46 cm below the position of the initial BEC, and we record the time and transverse position of each atomic impact with a detection efficiency $\eta \approx 25\%$ (Methods). The time of flight to the detector is approximately 300 ms, long enough for the recorded signal to yield the three components of the atomic velocity. By collecting data from several hundred repetitions of the experiment under the same conditions, we are able to reconstruct all desired atom number correlations within variable integration volumes of extent $\Delta v_z \times \Delta v_\perp^2$. These volumes play a similar role to that of the spatial and spectral filters in the HOM experiment and can be adjusted to erase the information that could allow tracing back the origin of a detected particle to one of the input channels.

The HOM dip should appear in the cross-correlation between the detection signals in the output channels of the beam-splitter¹⁶ (see also Methods), $G_{cd}^{(2)}$:

$$G_{cd}^{(2)} = \left(\frac{\eta}{\Delta v_z \Delta v_\perp^2} \right)^2 \iint \mathcal{V}_c \times \mathcal{V}_d \langle \hat{a}_{v_c}^\dagger \hat{a}_{v_d}^\dagger \hat{a}_{v_d} \hat{a}_{v_c} \rangle d^3 v_c d^3 v_d \quad (1)$$

Here, \hat{a}_v and \hat{a}_v^\dagger denote the annihilation and creation operators of an atom with three-dimensional velocity \mathbf{v} , respectively, $\langle \cdot \rangle$ stands for the quantum and statistical average and $\mathcal{V}_{c,d}$ designates the integration volumes centred on the output atom beams c and d (Fig. 1c). We have measured this correlation as a function of the duration of propagation $\tau = t_3 - t_2$ between the mirror and the beam-splitter (Fig. 3) and for various integration volumes (see Methods and Extended Data Fig. 1). We observe a marked reduction of the correlation when τ is equal to the duration of propagation from the source to the mirror ($t_3 - t_2 \approx t_2 - t_1$) and for small enough integration volumes, corresponding to a

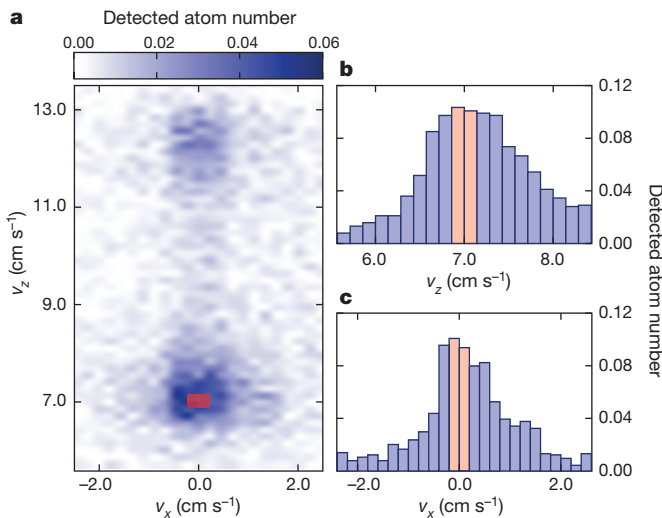


Figure 2 | Velocity distribution of the twin atoms. **a**, Two-dimensional velocity distribution of the twin atom beams emitted by the source. The red shaded area, drawn here only for the lower beam, labelled b in Fig. 1b and c, shows the integration volume \mathcal{V}_b used for computing the correlation function displayed in Fig. 3. The distribution corresponds to an average over about 1,100 measurements and is not corrected for the limited detection efficiency. The velocities are given relative to the laboratory frame of reference. The size of each pixel is 0.24 cm s^{-1} in the transverse directions (x and y) and 0.14 cm s^{-1} in the longitudinal (z) direction and an integration over 2 pixels is performed along the y direction. **b**, **c**, Cuts of the two-dimensional velocity distribution through the centre of the lower beam along the longitudinal (**b**) and transverse (**c**) directions. The data points result from the average over 2 pixels along the direction perpendicular to the cut. The red shaded area again shows the integration volume.

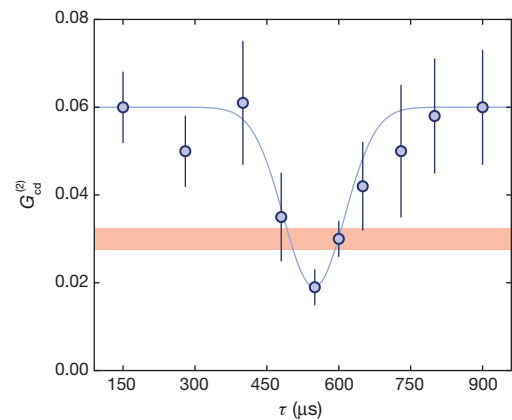


Figure 3 | HOM dip in the cross-correlation function. The correlation $G_{cd}^{(2)}$ between the output channels of the beam-splitter, defined in equation (1), was measured as a function of the duration of propagation $\tau = t_3 - t_2$ between the mirror and the beam splitter. The HOM dip is directly visible as a marked reduction of the correlation when τ approximately equals the duration of propagation between the source and the mirror, $t_2 - t_1 \approx 500\ \mu\text{s}$. This situation corresponds to symmetric paths between the source and the beam-splitter, that is, when one cannot distinguish between the two diagrams of Fig. 1c. A Gaussian fit (blue line) precisely locates the dip at $\tau = 550(50)\ \mu\text{s}$, with a full-width at half-maximum of $150(40)\ \mu\text{s}$, where the uncertainty corresponds to the 68% confidence interval. The fitted value of the background correlation is $0.060(5)$ and the measured visibility is $V = 0.65(7)$. It is two standard deviations beyond the classical-to-quantum threshold represented by the red shaded area, at half the background correlation value. Each data point was obtained from an average over about 500 to 1,400 repetitions of the experiment. Error bars denote the standard deviation of the statistical ensemble. The mean detected atom number was constant over the range of values of τ displayed here (see Methods and Extended Data Fig. 2).

full overlap of the atomic wave-packets on the beam-splitter. Fitting the data with an empirical Gaussian profile yields a visibility:

$$V = \frac{\max_{\tau} G_{cd}^{(2)}(\tau) - \min_{\tau} G_{cd}^{(2)}(\tau)}{\max_{\tau} G_{cd}^{(2)}(\tau)} = 0.65(7) \quad (2)$$

where the number in parenthesis stands for the 68% confidence interval. As we shrink the integration volumes, we observe that the dip visibility first increases and then reaches a saturation value, as is expected when the integration volumes become smaller than the elementary atomic modes. The data displayed in Fig. 3 were obtained for $\Delta v_z = 0.28 \text{ cm s}^{-1}$ and $\Delta v_{\perp} = 0.48 \text{ cm s}^{-1}$, which maximizes the reduction of the correlation while preserving a statistically significant number of detection events (see Methods and Extended Data Fig. 1).

The dip in the cross-correlation function cannot be explained in terms of classical particles, for which we would have no correlation at all between the detections in the output channels (Methods). But when the atoms are viewed as waves, demonstrating the quantum origin of the dip necessitates a deeper analysis. The reason is that two waves can interfere at a beam-splitter and give rise to an intensity imbalance between the output channels. If, in addition, the coherence time of the waves is finite, the cross-correlation can display a dip similar to the one observed in our experiment. But once averaged over the phase difference between the beams, the classical visibility is bounded from above and cannot exceed 0.5 (ref. 26 and Methods). In our experiment, this phase difference is randomized by the shot-to-shot fluctuations of the relative phase between the laser beams used for Bragg diffraction (Methods). Since our measured visibility exceeds the limit for waves by two standard deviations, we can safely rule out any interpretation of our observation in terms of interference between two ‘classical’ matter waves or, in other words, between two ordinary wave functions describing each of the two particles separately.

Two contributions may be responsible for the non-zero value of the correlation function at the centre of the dip: the detected particles may not be fully indistinguishable and the number of particles contained in the integration volume may exceed unity for each beam (see Methods). The effect of the atom number distribution can be quantified by measuring the intensity correlations of the twin atom beams upstream of the beam-splitter (Fig. 1c), which bound the visibility of the dip through the relation:

$$V_{\max} = 1 - \frac{G_{aa}^{(2)} + G_{bb}^{(2)}}{G_{aa}^{(2)} + G_{bb}^{(2)} + 2G_{ab}^{(2)}} \quad (3)$$

where $G_{aa}^{(2)}$, $G_{bb}^{(2)}$ and $G_{ab}^{(2)}$ are defined by analogy to equation (1) (ref. 26 and Methods) and the integration volumes $\mathcal{V}_{a,b}$ have the same extent as $\mathcal{V}_{c,d}$. Here, one immediately sees that the finite probability of having more than one atom per input channel, which translates to finite values of the auto-correlations $G_{aa}^{(2)}$, $G_{bb}^{(2)}$, leads to a reduced visibility. We have performed the measurement of these correlations following the same experimental procedure as before, except that we did not apply the mirror and beam-splitter. We find non-zero values $G_{aa}^{(2)} = 0.016(5)$, $G_{bb}^{(2)} = 0.047(9)$, and $G_{ab}^{(2)} = 0.048(7)$, yielding $V_{\max} = 0.60(10)$, where the uncertainty is the standard deviation of the statistical ensemble. Because of the good agreement with the measured value of the visibility, we conclude that the atom number distribution in the input channels entirely accounts for the visibility of the HOM dip. For the present experiment, we estimate the average number of incident atoms to be 0.5(1) in \mathcal{V}_a and 0.8(2) in \mathcal{V}_b , corresponding to a ratio of the probability for having two atoms to that for having one atom of 0.25(5) and 0.40(10), respectively (Methods). Achieving much smaller values is possible, for instance by reducing the pair production rate, but at the cost of lower counting statistics.

Although multiparticle interference can be observed with independently prepared photons^{27,28}, atoms¹³ and electrons^{29,30}, twin particle sources are at the heart of many protocols for quantum information

processing¹⁴ and quantum simulation¹⁵. The good visibility of the HOM dip in our experiment demonstrates that our twin atom source produces beams that have highly correlated populations and are well mode matched. This is an important achievement in itself, which may have the same impact on quantum atom optics as the development of twin photon sources using nonlinear crystals had for quantum optics.

Online Content Methods, along with any additional Extended Data display items and Source Data, are available in the online version of the paper; references unique to these sections appear only in the online paper.

Received 9 November 2014; accepted 6 February 2015.

- Bell, J. S. On the Einstein-Podolsky-Rosen paradox. *Physics* **1**, 195–200 (1964).
- Aspect, A. Bell’s inequality test: more ideal than ever. *Nature* **398**, 189–190 (1999).
- Giustina, M. *et al.* Bell violation using entangled photons without the fair-sampling assumption. *Nature* **497**, 227–230 (2013).
- Christensen, B. G. *et al.* Detection-loophole-free test of quantum nonlocality, and applications. *Phys. Rev. Lett.* **111**, 130406 (2013).
- Hong, C. K., Ou, Z. Y. & Mandel, L. Measurement of subpicosecond time intervals between two photons by interference. *Phys. Rev. Lett.* **59**, 2044–2046 (1987).
- Rarity, J. G. & Tapster, P. R. Experimental violation of Bell’s inequality based on phase and momentum. *Phys. Rev. Lett.* **64**, 2495–2498 (1990).
- Lewis-Swan, R. J. & Kheruntsyan, K. V. Motional-state Bell inequality test with ultracold atoms. Preprint at <http://arXiv.org/abs/1411.0191> (2014).
- Penrose, R. Quantum computation, entanglement and state reduction. *Phil. Trans. R. Soc. Lond. A* **356**, 1927–1939 (1998).
- Zurek, W. H. Decoherence, einselection, and the quantum origins of the classical. *Rev. Mod. Phys.* **75**, 715–775 (2003).
- Schlosshauer, M. Decoherence, the measurement problem, and interpretations of quantum mechanics. *Rev. Mod. Phys.* **76**, 1267–1305 (2005).
- Leggett, A. J. How far do EPR-Bell experiments constrain physical collapse theories? *J. Phys. A* **40**, 3141–3149 (2007).
- Bücker, R. *et al.* Twin-atom beams. *Nature Phys.* **7**, 608–611 (2011).
- Kaufman, A. M. *et al.* Two-particle quantum interference in tunnel-coupled optical tweezers. *Science* **345**, 306–309 (2014).
- Nielsen, M. A. & Chuang, I. L. *Quantum Computation and Quantum Information* (Cambridge Univ. Press, 2000).
- Kitagawa, T., Aspect, A., Greiner, M. & Demler, E. Phase-sensitive measurements of order parameters for ultracold atoms through two-particle interferometry. *Phys. Rev. Lett.* **106**, 115302 (2011).
- Ou, Z. Y. *Multi-Photon Quantum Interference* (Springer, 2007).
- Grynberg, G., Aspect, A. & Fabre, C. *Introduction to Quantum Optics: From the Semiclassical Approach to Quantized Light* (Cambridge Univ. Press, 2010).
- Bonneau, M. *et al.* Tunable source of correlated atom beams. *Phys. Rev. A* **87**, 061603 (2013).
- Cronin, A. D., Schmiedmayer, J. & Pritchard, D. E. Optics and interferometry with atoms and molecules. *Rev. Mod. Phys.* **81**, 1051–1129 (2009).
- Schellekens, M. *et al.* Hanbury Brown Twiss effect for ultracold quantum gases. *Science* **310**, 648–651 (2005).
- Hilligsøe, K. M. & Mølmer, K. Phase-matched four-wave mixing and quantum beam splitting of matter waves in a periodic potential. *Phys. Rev. A* **71**, 041602 (2005).
- Campbell, G. K. *et al.* Parametric amplification of scattered atom pairs. *Phys. Rev. Lett.* **96**, 020406 (2006).
- Gross, C. *et al.* Atomic homodyne detection of continuous-variable entangled twin-atom states. *Nature* **480**, 219–223 (2011).
- Lücke, B. *et al.* Twin matter waves for interferometry beyond the classical limit. *Science* **334**, 773–776 (2011).
- Bookjans, E., Hamley, C. & Chapman, M. Strong quantum spin correlations observed in atomic spin mixing. *Phys. Rev. Lett.* **107**, 210406 (2011).
- Lewis-Swan, R. J. & Kheruntsyan, K. V. Proposal for demonstrating the Hong–Ou–Mandel effect with matter waves. *Nature Commun.* **5**, 3752 (2014).
- Beugnon, J. *et al.* Quantum interference between two single photons emitted by independently trapped atoms. *Nature* **440**, 779–782 (2006).
- Lang, C. *et al.* Correlations, indistinguishability and entanglement in Hong–Ou–Mandel experiments at microwave frequencies. *Nature Phys.* **9**, 345–348 (2013).
- Bocquillon, E. *et al.* Coherence and indistinguishability of single electrons emitted by independent sources. *Science* **339**, 1054–1057 (2013).
- Dubois, J. *et al.* Minimal-excitation states for electron quantum optics using levitons. *Nature* **502**, 659–663 (2013).

Acknowledgements We thank J. Ruaudel and M. Bonneau for contributions to the early steps of the experiment. We also thank K. Kheruntsyan, J. Chwedeńczuk and P. Deuar for discussions. We acknowledge funding by IFRAF, Triangle de la Physique, Labex PALM, ANR (PROQUP, QEAGE), FCT (scholarship SFRH/BD/74352/2010 co-financed by ESF, POPH/QREN and EU to R.L.) and EU (ERC grant 267775, QUANTATOP, and Marie Curie CIG 618760, CORENT).

Author Contributions All authors contributed extensively to this work.

Author Information Reprints and permissions information is available at www.nature.com/reprints. The authors declare no competing financial interests. Readers are welcome to comment on the online version of the paper. Correspondence and requests for materials should be addressed to R.L. (raphael.lobes@institutoptique.fr) or M.C. (marc.cheneau@institutoptique.fr).

METHODS

Twin atom source. The twin atom beams result from a scattering process between pairs of atoms from the BEC occurring when the gas is placed in a moving one-dimensional optical lattice. The use of a BEC is dictated primarily by the need to maximize the atomic density to assure a sufficiently high scattering rate. The experimental set-up has been described in ref. 18. The lattice is formed by two laser beams derived from the same source emitting at the wavelength $\lambda = 1,064$ nm. In contrast to our previous work, the axis of the optical lattice was now precisely aligned with the long axis of the optical trap confining the atoms. The laser beams intersect with an angle of $\theta = 166^\circ$, their frequency difference is set to 100.5 kHz and the lattice depth to $0.8 E_{\text{rec}}$ (see below). This constrains the longitudinal wave vector of the twin atoms to the values $k_{z,a} = 0.75 k_{\text{rec}}$ and $k_{z,b} = 1.30 k_{\text{rec}}$ in order to fulfil the conservation of quasi-momentum and energy in the frame co-propagating with the lattice. Here, $k_{\text{rec}} = 2\pi \sin(\theta/2)/\lambda$ is the recoil wave vector along the longitudinal axis gained upon absorption of a photon from a lattice laser and $E_{\text{rec}} = \hbar^2 k_{\text{rec}}^2 / 2m$ is the associated kinetic energy, with \hbar the reduced Planck constant and $m = 6.64 \times 10^{-27}$ kg the mass of a ^4He atom. The observed velocities of the twin atom beams coincide with the expected values above, using the relation $v = \hbar k / m$. The optical lattice is turned on and off adiabatically so as to avoid diffraction of the atoms during this phase of the experiment. The relative velocities of the pair is such that during the interferometer sequence, the maximum separation of the beams is only 25 μm , smaller than the size of the clouds. This separation, however, plays no role in the experiment; we need only ensure that the atoms in a pair are distinguishable by some observable, in our case the momentum. Thus a second reason to use a BEC in the experiment is to benefit from its narrow momentum distribution, which results in well separated pairs in momentum space.

Transfer to the magnetically insensitive internal state. Transfer to the $m = 0$ state after the optical trap has been switched off is made necessary by the presence of stray magnetic fields in the vacuum chamber that otherwise would lead to a severe deformation of the atomic distribution during the long free fall. The transfer is achieved by introducing a two-photon coupling between the $m = 1$ state, in which the atoms are initially, and the $m = 0$ state using two laser beams derived from a single source emitting at 1,083 nm and detuned by 600 MHz from the 2^3S_1 to 2^3P_0 transition. The frequency difference of the laser beams is chirped across the two-photon resonance so as to realize an adiabatic fast passage transition (the frequency change is 300 kHz in 300 μs). We have measured the fraction of transferred atoms to be 94%. The remaining 6% stay in the $m = 1$ state and are pushed away from the integration volumes by stray magnetic field gradients.

Atomic mirror and beam-splitter. The mirror and beam-splitter are both implemented using Bragg scattering on a second optical lattice. This effect can be seen as a momentum exchange between the atoms and the laser beams forming the lattice, a photon being coherently absorbed from one beam and emitted into the other. In our experiment, the laser beams forming the lattice have a waist of 1 mm and are detuned by 600 MHz from the 2^3S_1 to 2^3P_0 transition (they are derived from the same source as the beams used for the Raman transfer). In order to fulfil the Bragg resonance condition for the atom beams, the laser beams are made to intersect at an angle of 32° and the frequency of one of the beams is shifted by 57 kHz. In addition to this fixed frequency difference, a frequency chirp is performed to compensate for the acceleration of the atoms during their free fall. The interaction time between the atoms and the optical lattice was 100 μs for the mirror operation (π -pulse) and 50 μs for the beam-splitter operation ($\pi/2$ -pulse). The resonance condition for the momentum state transfer is satisfied by all atoms in the twin beams but only pairs of states with a well defined momentum difference are coupled with each other. We measured the reflectivity of the mirror and the transmittance of the beam-splitter to be 0.95(2) and 0.49(2), respectively. Spontaneous scattering of photons by the atoms was negligible.

Interactions between atoms can alter the effect of the beam-splitter³¹. In our experiment, however, the atomic density at the beam-splitter is so low that the frequency associated with the typical interparticle interaction energy is more than 3 orders of magnitude smaller than the inverse of the time it takes for Bragg scattering to take place. Thus particle interactions are negligible during the beam splitting process.

Detection efficiency. Our experiment relies on the ability to detect the atoms individually. The detection efficiency is an essential parameter for achieving good signal to noise ratios, although it does not directly influence the visibility of the HOM dip. Our most recent estimate of the detection efficiency relies on the measurement of the variance of the atom number difference between the twin beams. For this we use the same procedure as described in ref. 18, but with an integration volume that includes the entire velocity distribution of each beam. We find a normalized variance of 0.75(5), well below the Poissonian floor. Since for perfectly correlated twin beams the measured variance would be $1 - \eta$, we attribute the lower limit of 25(5)% to our detection efficiency. This value for η is a factor of about 2 larger than the lower bound quoted in ref. 32. The difference is due to the change of method employed for

transferring the atoms from the $m = 1$ to the $m = 0$ state after the optical trap has been switched off. We previously used a radio-frequency transfer with roughly 50% efficiency whereas the current optical Raman transfer has close to 100% efficiency.

Distribution of the number of incident atoms. We have estimated the average number of incident atoms in each input channel of the beam-splitter, n_a and n_b , by analysing the distribution of detected atoms in the integration volumes \mathcal{V}_a and \mathcal{V}_b . We fitted these distributions by assuming an empirical Poissonian law for the distribution of incident atoms and taking into account the independently calibrated detection efficiency. The values of n_a and n_b given in the main text are the mean values of the Poissonian distributions that best fit the data. The probabilities for having one or two atoms in each of the input channels of the beam-splitter was obtained from the same analysis. The uncertainty on these numbers mostly stems from the uncertainty on the detection efficiency.

The HOM effect. The HOM effect appears in the correlator $\langle \hat{a}_c^\dagger \hat{a}_d^\dagger \hat{a}_c \hat{a}_d \rangle$ of equation (1). The simplest way to calculate such a correlator is to transform the operators and the state vector back in the input space before the beam-splitter and to use the Heisenberg picture. The transformation matrix between the operators $\hat{a}_c(t_3)$, $\hat{a}_d(t_3)$ and $\hat{a}_v(t_3)$, $\hat{a}_w(t_3)$ can be worked out from first principles. For the Bragg beam-splitter, and using a Rabi two-state formalism, we find:

$$\begin{cases} \hat{a}_c = \frac{1}{\sqrt{2}} (i e^{i\phi} \hat{a}_v + \hat{a}_w) \\ \hat{a}_d = \frac{1}{\sqrt{2}} (\hat{a}_v + i e^{-i\phi} \hat{a}_w) \end{cases}$$

where ϕ is the relative phase between the laser beams forming the optical lattice. In the ideal case of an input state with exactly one atom in each channel, $|1_{v_a}, 1_{v_b}\rangle$, we therefore obtain:

$$\begin{aligned} \|\hat{a}_v \hat{a}_w |1_{v_a}, 1_{v_b}\rangle\|^2 &= \frac{1}{4} \left\| \left(i e^{i\phi} \hat{a}_v^2 + i e^{-i\phi} \hat{a}_w^2 + \hat{a}_v \hat{a}_w + i^2 \hat{a}_w \hat{a}_v \right) |1_{v_a}, 1_{v_b}\rangle \right\|^2 \\ &= \frac{1}{4} \|0 + (1 + i^2) |0_{v_a}, 0_{v_b}\rangle\|^2 \\ &= 0 \end{aligned}$$

meaning that the probability of joint detection is strictly zero. (Here we use $\|\dots\|$ to indicate vector norm.) The detailed calculation above makes clear that the perfect destructive interference between the two-particle state amplitudes associated with the two diagrams of Fig. 1c is at the heart of the HOM effect. By contrast, input states containing more than one atom per channel are transformed into a sum of orthogonal states and the interference can only be partial. Taking $|2_{v_a}, 2_{v_b}\rangle$, for instance, yields:

$$\begin{aligned} \|\hat{a}_v \hat{a}_w |2_{v_a}, 2_{v_b}\rangle\|^2 &= \frac{1}{4} \left\| \left(i e^{i\phi} \hat{a}_v^2 + i e^{-i\phi} \hat{a}_w^2 + \hat{a}_v \hat{a}_w + i^2 \hat{a}_w \hat{a}_v \right) |2_{v_a}, 2_{v_b}\rangle \right\|^2 \\ &= \frac{1}{2} \left\| i e^{i\phi} |0_{v_a}, 2_{v_b}\rangle + i e^{-i\phi} |2_{v_a}, 0_{v_b}\rangle + \sqrt{2}(1 + i^2) |1_{v_a}, 1_{v_b}\rangle \right\|^2 \\ &= \frac{1}{2} \left\| e^{i\phi} |0_{v_a}, 2_{v_b}\rangle + e^{-i\phi} |2_{v_a}, 0_{v_b}\rangle \right\|^2 \\ &= 1 \end{aligned}$$

Finally, we note that losses in one of the incident beams, for instance beam a, can be modelled by a fictitious beam-splitter with a transmission coefficient T . In the above calculation, these losses would therefore only manifest by an additional factor \sqrt{T} in front of every operator \hat{a}_v , leaving unaffected the destructive interference that gives rise to the HOM effect.

Stability of the atom number in the output ports. The mean detected atom number in the output ports c and d is plotted as a function of τ in Extended Data Fig. 2a and b. It remains constant within the statistical uncertainty, which confirms the interpretation of the dip as a destructive two-particle interference. To easily compare the atom number fluctuations with the variation of the cross-correlation across the HOM dip, the product of the averaged populations $\langle n_c \rangle \cdot \langle n_d \rangle$ and the cross-correlation $G_{cd}^{(2)}$ are displayed together as a function of τ in Extended Data Fig. 2c. In contrast to the cross-correlation, it is impossible to identify a marked reduction of $\langle n_c \rangle \cdot \langle n_d \rangle$ around $\tau = 550 \mu\text{s}$.

Influence of the integration volume on the dip visibility. The visibility of the HOM dip is plotted in Extended Data Fig. 1 as a function of the longitudinal (Extended Data Fig. 1a) and transverse (Extended Data Fig. 1b) integration volumes. The red dots identify the integration volume used in Fig. 3 of the main text and correspond to a compromise between signal-to-noise ratio and visibility amplitude. As we shrink the integration volumes, the dip visibility first increases and then reaches a saturation value, meaning that the integration volume becomes smaller than the elementary atomic modes³³⁻³⁵. Reducing further the integration volume only leads to an increase of the statistical uncertainty.

The visibility V is obtained by fitting the cross-correlation function $G_{cd}^{(2)}(\tau)$ measured in the experiment with the empirical function:

$$f(\tau) = G_{bg}^{(2)} (1 - V \exp(-(\tau - \tau_0)^2 / 2\sigma^2))$$

where the background correlation $G_{bg}^{(2)}$, the centre of the dip τ_0 and the width of the dip σ are all left as free parameters.

Visibility of the HOM dip. A slightly less general form of equation (3) has been derived in ref. 26 assuming a two-mode squeezed state as an input state. The same calculation can be performed for an arbitrary input state. Leaving aside the integration over the velocity distribution, we find that the cross-correlation for indistinguishable particles can be expressed as:

$$G_{cd}^{(2)} \Big|_{\text{indisc.}} = \frac{1}{4} (G_{aa}^{(2)} + G_{bb}^{(2)} + \mathcal{A}) \quad , \quad \mathcal{A} = 2\eta^2 \text{Re} \left[e^{2i\phi} \langle \hat{a}_{v_a}^\dagger \hat{a}_{v_a}^\dagger \hat{a}_{v_b} \hat{a}_{v_b} \rangle \right]$$

whereas that of distinguishable particles reads:

$$G_{cd}^{(2)} \Big|_{\text{disc.}} = \frac{1}{4} (G_{aa}^{(2)} + G_{bb}^{(2)} + 2G_{ab}^{(2)})$$

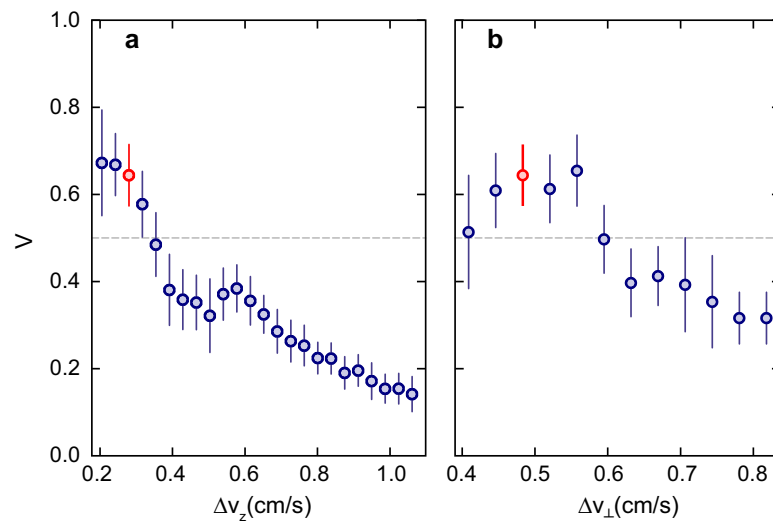
Here, the correlators appearing in the right-hand side are taken at time t_1 , that is, immediately after the atom beams have been produced. The term \mathcal{A} corresponds to an interference between single-particle matter waves. It depends on both the relative phase between the atom beams and the relative phase between the laser beams used for Bragg diffraction. The latter is counted once for the atomic mirror and once for the atomic beam-splitter. Twin beams with perfect correlations in their population would have a fully random relative phase. In our experiment however, the population imbalance between the atom beams could entail a residual phase coherence. Instead, the relative phase between the laser beams was left uncontrolled and

its value was randomly distributed between two repetitions of the experiment. As a result, the term \mathcal{A} must average to zero and the visibility of the HOM dip be given by equation (3), as observed in the experiment. Following ref. 26, we also note that equation (3) yields the ultimate bound for waves interfering on the beam-splitter:

because waves must fulfil the Cauchy–Schwarz inequality, $G_{ab}^{(2)} < \sqrt{G_{aa}^{(2)} G_{bb}^{(2)}}$, the visibility of the classical dip cannot exceed 0.5 (ref. 36).

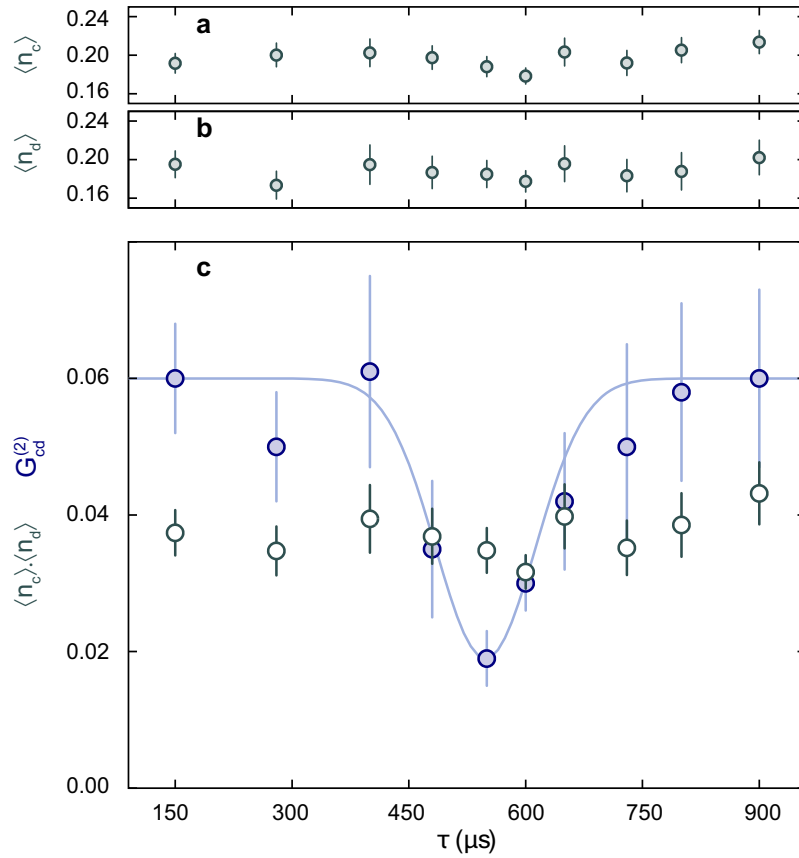
The above results hold true for a finite integration over the atomic velocity distribution provided that two conditions are met: (1) it must remain impossible to distinguish the atoms entering the beam-splitter through channel a from the atoms entering through channel b once they have exited the beam-splitter; (2) the transformation matrix of the beam-splitter must keep the same form after integration. In our experiment, the second condition is naturally satisfied because the Bragg diffraction only couples atomic states with a well defined momentum difference and we fulfil the first condition by reducing the integration volume as much as it is necessary.

31. Andersson, E., Fontenelle, M. & Stenholm, S. Quantum statistics of atoms in microstructures. *Phys. Rev. A* **59**, 3841–3850 (1999).
32. Jaskula, J.-C. *et al.* Sub-Poissonian number differences in four-wave mixing of matter waves. *Phys. Rev. Lett.* **105**, 190402 (2010).
33. Rarity, J. G. & Tapster, P. R. Fourth-order interference in parametric downconversion. *J. Opt. Soc. Am. B* **6**, 1221–1226 (1989).
34. Treps, N., Delaubert, V., Maître, A., Courty, J. M. & Fabre, C. Quantum noise in multipixel image processing. *Phys. Rev. A* **71**, 013820 (2005).
35. Morizur, J.-F., Armstrong, S., Treps, N., Janousek, J. & Bachor, H.-A. Spatial reshaping of a squeezed state of light. *Eur. Phys. J. D* **61**, 237–239 (2011).
36. Ou, Z. Y. Quantum theory of fourth-order interference. *Phys. Rev. A* **37**, 1607–1619 (1988).



Extended Data Figure 1 | HOM dip visibility as a function of the integration volumes. **a**, Visibility V as a function of the longitudinal integration interval Δv_z . The transverse integration interval is kept constant at $\Delta v_\perp = 0.48 \text{ cm s}^{-1}$. **b**, Visibility as a function of the transverse integration

interval Δv_\perp . The longitudinal integration interval is kept constant at $\Delta v_z = 0.28 \text{ cm s}^{-1}$. The red points mark the values discussed in the main text. Error bars denote the standard deviation of the statistical ensemble.



Extended Data Figure 2 | Averaged number of incident atoms over the HOM dip. **a**, Averaged atom number detected in \mathcal{V}_c , n_c , as a function of the propagation time τ . The mean value of $n_c(\tau)$ is 0.20 with a standard deviation of 0.01. **b**, Averaged atom number detected in \mathcal{V}_d , n_d , as a function of the

propagation time τ . The mean value of $n_d(\tau)$ is 0.19 with a standard deviation of 0.01. **c**, The cross-correlation between the output ports c and d (solid blue circles), displaying the HOM dip, is compared to $\langle n_c \rangle \cdot \langle n_d \rangle$ (open grey circles). Error bars denote the standard deviation of the statistical ensemble.